China Ocean Eng., 2017, Vol. 31, No. 3, P. 308–316
DOI: 10.1007/s13344-017-0036-z, ISSN 0890-5487
http://www.chinaoceanengin.cn/ E-mail: coe@nhri.cn

Experimental Study on the Bed Shear Stress Under Breaking Waves

HAO Si-yu[a, b, c, d, *], XIA Yun-feng[a, c, d], XU Hua[a, c, d]

[a]Nanjing Hydraulic Research Institute, Nanjing 210029, China

[b]College of Harbor, Coastal and Offshore Engineering, Hohai University, Nanjing 210098, China

[c]The State Key Laboratory of Hydrology-Water Resources and Hydraulic Engineering, Nanjing 210098, China

[d]Key Laboratory of Port, Waterway and Sedimentation Engineering of Ministry of Transport, Nanjing 210024, China

Received March 3, 2017; revised April 26, 2017; accepted May 5, 2017

Abstract

The object of present study is to investigate the bed shear stress on a slope under regular breaking waves by a novel instrument named Micro-Electro-Mechanical System (MEMS) flexible hot-film shear stress sensor. The sensors were calibrated before application, and then a wave flume experiment was conducted to study the bed shear stress for the case of regular waves spilling and plunging on a 1:15 smooth PVC slope. The experiment shows that the sensor is feasible for the measurement of the bed shear stress under breaking waves. For regular incident waves, the bed shear stress is mainly periodic in both outside and inside the breaking point. The fluctuations of the bed shear stress increase significantly after waves breaking due to the turbulence and vortexes generated by breaking waves. For plunging breaker, the extreme value of the mean maximum bed shear stress appears after the plunging point, and the more violent the wave breaks, the more dramatic increase of the maximum bed shear stress will occur. For spilling breaker, the increase of the maximum bed shear stress along the slope is gradual compared with the plunging breaker. At last, an empirical equation about the relationship between the maximum bed shear stress and the surf similarity parameter is given, which can be used to estimate the maximum bed shear stress under breaking waves in practice.

Key words: bed shear stress, direct measurement, shear stress sensor, spilling breaker, plunging breaker

Citation: Hao, S. Y., Xia, Y. F., Xu, H., 2017. Experimental study on bed shear stress under breaking waves. China Ocean Eng., 31(3): 308–316, doi: 10.1007/s13344-017-0036-z

1 Introduction

Surf zone is the most active area for sediment transport and beach morphology in the nearshore region, and wave breaking is the most typical hydrodynamics in the surf zone. The bed shear stress directly dominates the sediment movement. In research and engineering application of sediment transport, the bed shear stress is a key quantity to estimate the threshold motion of sediment, bedload transport, and reference concentration of pick-up rate for sediment to suspension (Soulsby, 1997). Therefore, the investigation on the bed shear stress under breaking waves is significant to reveal the mechanics of sediment transport in the surf zone. However, due to the small order of magnitude and quick change of the bed shear stress in the wave boundary layer, direct and accurate measurement of the bed shear stress in such circumstance remains a challenge nowadays.

An instrument commonly used to measure the wave bed shear stress directly is a flush-mounted shear plate. The bed shear stress is calculated by measuring the displacement of the shear plate or the force applied to it. Mirfenderesk and Young (2003) directly measured the bed shear stress by the shear plate on the smooth and rough bed under wave action. The shear plates used in bed shear stress measurement under wave action were also developed by Huo et al. (2007), You and Yin (2007), and Huang et al. (2016). By using a shear plate, Barnes et al. (2009) measured the bed shear stress in the swash zone, and Seelam et al. (2011) measured the bed shear stress under solitary waves. Under wave action, the horizontal force acting on the shear plate consists of the bed shear stress on the surface of the plate and the wave pressure gradient between the front and rear edge of the plate. Pujara and Liu (2014) designed a shear plate considering the existence of pressure gradient. Other than the pressure gradient issue, the size of the shear plate will also affect the spatial resolution because the bed shear stress is the average shear stress acted on the surface of the shear plate. The shear plate still has its advantages in the measurement of a wet-dry alternating region and rough bed. Anoth-

Foundation item: This study was financially supported by the National Key Scientific Instrument and Equipment Development Project (Grant No. 2013YQ04091108) and the National Natural Science Foundation of China (Grant No. 51309158).

*Corresponding author. E-mail: haosiyu@whu.edu.cn

er conventional measuring instrument is the flush-mounted hot-film probe whose operating principle is heat transfer. Sumer et al. (1993) developed a two-component hot-film probe driven by constant temperature anemometer and attempted to measure the wave bed shear stress along with detection of the direction. One a dvantage of a hot-film probe compared with the shear plate is its ability to obtain high-frequency fluctuating characteristics, so that it is used in the study of the wave boundary layer (e.g. Jensen et al., 1989; Carstensen et al., 2010). Because the size of the hot-film probe is smaller than the shear plate, the hot-film has a higher spatial resolution than the shear plate. However, the small size will bring alignment problem while mounting the probe. Unaligned flush mounting of the hot-film probe will lead to inaccurate measurement. When mounted on a curved surface, the discontinuity between the hot-film probe and surface is also an existing problem.

Recently, some new types of bed shear stress sensors have appeared. Musumeci et al. (2015) presented a novel direct measurement strategy of the wave bed shear stress based on the displacement of ferrofluid spike. With the development of Micro-Electro-Mechanical System (MEMS), the MEMS flexible hot-film shear stress sensor used in aerodynamic research has extended to the underwater measurements (Ma et al., 2010). Xu et al. (2015) used this sensor to measure the bed shear stress under wave-current interaction in a wave flume. The main advantages of this sensor are its high temporal and spatial resolution, which are suitable for wave application. Compared with the flush-mounted hot-film probe, there is no alignment issue in installing the sensor, and the flexible film sensor can be directly pasted to the surface including the curved one.

Fredsøe et al. (2003) have studied the influence of externally generated turbulence on the bed shear stress in an oscillating water tunnel. In the surf zone, wave breaking will generate turbulence and vortexes, which may penetrate into the wave boundary layer. The influence of wave breaking on the bed shear stress on a slope has not been well understood yet. The shear plate widely used in the study of the wave bed shear stress can be applied in the surf zone. Boers (2005) used the shear plate to measure the bed shear stress on a barred beach in the surf zone. The flush-mounted hot-film probe is also used to measure the bed shear stress on a slope under breaking waves. Deigaard et al. (1991) measured the bed shear stress under spilling breaker and weak plunging breaker on a smooth and constant-slope bed using a flush-mounted hot-film probe. Yüksel et al. (1998) used this type probe measured the bed shear stress distribution on a steel beach. Sumer et al. (2011, 2013) conducted detailed bed shear measurement on a constant slope under plunging solitary wave and regular waves using this type probe with the assist of Laser Doppler Velocimetry (LDV) to determine the direction. An indirect method to obtain bed shear stress is to calculate the friction velocity by the velocity profile. Based on the found of a logarithmic velocity profile within the wave boundary layer for most of the phase over a wave period, Cox et al. (1996) used LDV to measure the velocity and then estimated the bed shear stress in the surf zone in the case of spilling breaker. Because it is difficult to accurately measure the velocity profile in the thin wave boundary layer and not the complete phase of the velocity profile fulfills the logarithmic distribution, this method has its drawback under violent breaking waves such like plunging breaker.

As described above, direct measurement of the bed shear stress under breaking waves is rarely reported due to the lack of accurate and effective measurement means. The purpose of present study is to investigate the bed shear stress under breaking waves. In present study, direct measurement of the bed shear stress is made by the MEMS flexible hot-film shear stress sensor which is a revised sensor used by Xu et al. (2015). The shear stress sensor is calibrated before application, and then the time series and the distribution of the bed shear stress along the slope for the case of both waves spilling and plunging which are commonly seen on the natural beach are investigated and compared. Finally, an empirical equation about the relationship between the maximum bed shear stress and the surf similarity parameter is given based on the measured data.

2 Instrument for bed shear stress measurement

2.1 MEMS flexible hot-film shear stress sensor

The MEMS flexible hot-film shear stress sensor is developed by Key Laboratory of Micro/Nano System for Aerospace, Northwestern Polytechnical University, China. Fig. 1 shows the shear stress sensor and its operating principle. The thermal unit of a shear stress sensor is fabricated

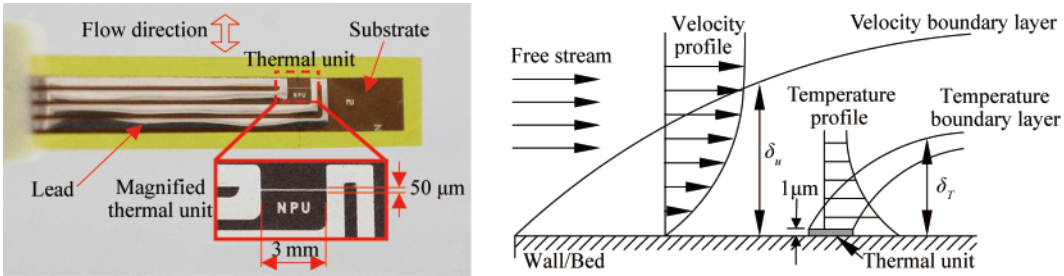

Fig. 1. MEMS flexible hot-film shear stress sensor and its operating principle underwater.

from nickel, and its size is only 1 μm thick, 50 μm wide, and 3 mm long. The sensor is so called hot-film shear stress sensor because the thermal unit is in the form of "film" attached on the substrate. A Parylene coating is deposited on the sensor to protect the sensor and insulate the sensor from the measured medium.

The thermal unit is heated by the electric current. When the fluid above the thermal unit flows, the forced heat convection will remove the heat from the thermal unit. Since the thermal unit is temperature-sensitive, the change in temperature of the thermal unit can be obtained by detecting the change in the resistance of the thermal unit resistance through an electrical bridge, which is reflected in the form of voltage. Then, according to the heat balance and forced heat convection relationship, we can get the flow velocity, flow rate, and wall shear stress. For water medium at the room temperature, the velocity boundary layer δ_u is thicker than the temperature boundary layer δ_T (Schlichting and Gersten, 2017), hence the thermal change of the thermal unit will only represent the information within the velocity boundary layer (as shown in Fig. 1) and the sensor can be used to measure the wall shear stress for underwater application.

There are three driving modes for this type of thermal sensor, namely constant current (CC), constant temperature (CT), and constant voltage (CV) mode. In the CC mode, the current I in the sensor is maintained constant, and the change in resistance can be simply obtained from the measured voltage. The engineering prototype which drives and detects the MEMS flexible hot-film shear stress sensor is equipped with CC mode currently, and its output frequency can exceed 500 Hz.

2.2 Calibration of the shear stress sensor

Before the application of the shear stress sensor, an accurate calibration is needed. Thermal sensors are sensitive to ambient temperature (Hultmark and Smits, 2010), so the calibration should be conducted under different water temperature for the application in the wave flume later.

The shear stress sensor was calibrated in a high aspect ratio rectangular duct with the temperature control system so that the sensor is calibrated at different water temperature. The calibration section of the duct is 3 m in length, 2 cm in height, and 22 cm in width (Fig. 2). This calibration device is based on the principle of the relationship between the pressure gradient and the wall shear stress of the fully developed flow. Knight et al. (1984) have studied the shear stress distribution in the ducts with different aspect ratios and proposed the following equation to calculate the maximum wall shear stress on the center line of the upper and lower walls in a rectangular duct.

$$\tau_b = -1.025\frac{H_c}{2}\frac{\Delta p}{\Delta x}\left[1-\mathrm{e}^{-(2B_c/3H_c)^{0.95}}\right], \tag{1}$$

where τ_b is the wall/bed shear stress at the central line, $\Delta p/\Delta x$ is the mean pressure gradient along the duct which can be obtained from a micro-differential pressure transducer, H_c is the height of the duct, and B_c is the width of the duct.

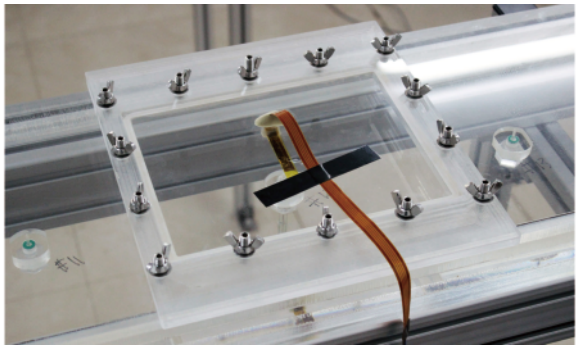

Fig. 2. Shear stress sensor installed at the calibration section of a rectangular duct.

For heat-transfer sensors, the classical calibration equation is as follows (Hanratty and Campbell, 1996):

$$\frac{I^2R}{\Delta T} = A(\rho\tau_b)^n + B, \tag{2}$$

where I is the current through the thermal unit, R is the resistance of the thermal unit, ΔT is the difference between the thermal unit temperature T_w and the ambient temperature T_a (namely the water temperature), and ρ is the water density. Parameters A, B, and n are the calibration coefficients that need to be determined through calibration experiments. For sensor working in the CC mode, according to Ohm's law E=IR where E is the output voltage, I and ΔT are constant in an instantaneous situation, and then Eq. (2) can be simplified as:

$$E = A\tau_b^n + B. \tag{3}$$

From Eqs. (1) and (3), the calibration coefficients A, B, and n can be determined at different water temperature for each sensor. Fig. 3 shows an example of the calibration curves at different water temperature. The output voltage decreases with the increase of the input shear stress at a certain temperature. This is because when the shear stress increases, which represents the flow velocity inside the boundary layer becomes larger, the effect of the forced heat

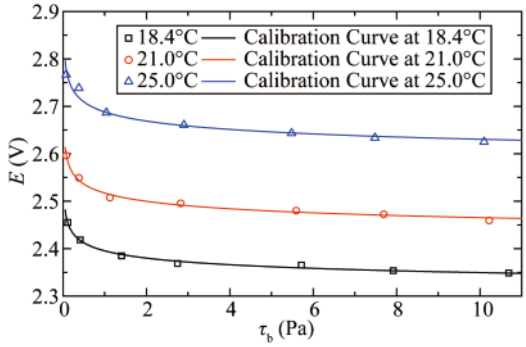

Fig. 3. Calibration curves of a shear stress sensor at different water temperature.

convection is strengthened, and then the heat dissipating ability of the thermal unit is enhanced. The temperature of the thermal unit becomes small so that the resistance also becomes small and the output voltage value will reduce accordingly. For different water temperature, the output voltage becomes higher when water temperature is higher. The reason is that as the ambient temperature increases, the initial operating temperature of the thermal unit also increases, resulting in an increase in the overall voltage. The calibration for different water temperatures is needed before its application, or additional recalibration can be performed after the application.

3 Experimental setup

3.1 Setup of the wave flume

The experimental measurement was conducted in a wave flume at Nanjing Hydraulic Research Institute. The setup of wave flume is shown in Fig. 4. The flume is 40 m in length, 0.8 m in width, and 1 m in depth. The periodic waves are generated by a piston-type wavemaker at one end. Because the sidewalls and bottom of the wave flume are toughened glass, to fix the experimental slope and avoid wave height attenuation in a long distance, a cement platform with the height of 20 cm was placed on the bottom at a distance of 14.5 m from the wavemaker. At a distance of 21.8 m from the wavemaker, a 1:15 experimental slope was constructed as a beach. The slope was made by smooth PVC plate and fastened to the cement platform by trusses with bolts. The joints of each PVC plate were sealed with silicone sealant, as well as the junctions between the sidewalls and the slope.

The measurement section of the bed shear stress on the slope is shown in Table 1. All the shear stress sensors were calibrated at different temperatures (20.7–21.5°C) measured in the wave flume using the method described in Section 2.2. The shear stress sensor was mounted along the slope together with the baseplate used in the calibration, and the joints between the baseplate and slope were dealt with in the same way described in the joints of each PVC plate before. The sampling rate of the engineering prototype was set at 500 Hz, and the measuring duration is 60 s.

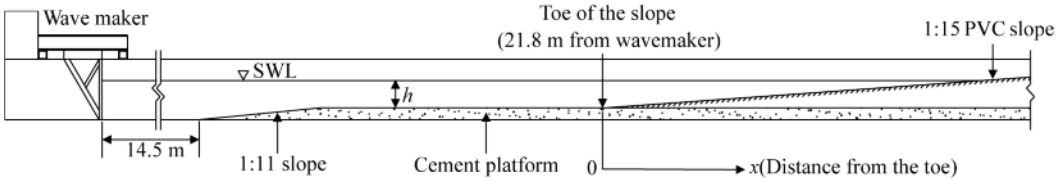

Fig. 4. Setup of wave flume for measurement of bed shear stress on a slope under breaking waves.

Table 1 Measurement sections of bed shear stress and velocity

Section/Sensor	A	B	C	D	E	F	G	H	I
Distance from toe (m)	2.23	2.66	3.10	3.53	3.96	4.82	5.26	5.69	6.12

The wave height was measured by conducting metric wave gauge that was developed by Nanjing Hydraulic Research Institute, and the sampling frequency was 50 Hz. A high-definition digital camera was installed next to the sidewall of wave flume to record the process. Because the shear stress sensor does not sense the direction of the bed shear stress, the velocity above the shear stress sensor was measured synchronously by Nortek Vectrino Acoustic Doppler Velocimeter (ADV) with a sampling frequency of 25 Hz. In this study, a down-looking probe was used, and the velocity measuring point was 5 cm far from the ADV probe. The velocity measuring point was 5 mm above the shear stress sensor.

3.2 Test conditions

In this study, the incident waves were regular waves, and the breaker type of wave is classified by the surf similarity parameter ξ_0, which is given as follows:

$$\xi_0 = \frac{\tan\beta}{\sqrt{H_0/L_0}}, \tag{4}$$

where $\tan\beta$ is the slope of the beach, H_0 is the deep-water wave height, and L_0 is the deep-water wavelength. Spilling breaker occurs when ξ_0 is smaller than 0.5, plunging breaker occurs when ξ_0 is between 0.5 and 3.3, and surging breaker occurs when ξ_0 larger than 3.3 (Galvin, 1968). The deep-water quantities are usually obtained by the back calculation from a measured wave height in the wave flume through linear wave theory. In the present experiment, the deep-water quantities were calculated from measured data at the toe of the slope.

Four test cases were conducted in the wave flume. The over all test conditions are given in Table 2 where h is the water depth at the toe of the slope, H is the wave height measured

Table 2 Test conditions for the bed shear stress measurement of breaking waves

Test case	$\tan\beta$	h(m)	H(cm)	T(s)	H_0(cm)	L_0(m)	ξ_0	Breaker type (classified)	Breaker type (observed)	x_b(m)
R1	1:15	0.45	8.0	3.0	7.2	14.04	0.934	Plunging	Plunging	4.63
R2	1:15	0.45	10.0	2.0	10.3	6.24	0.519	Plunging	Plunging	4.39
R3	1:15	0.45	13.6	1.0	14.4	1.56	0.219	Spilling	Spilling	3.87
R4	1:15	0.35	9.6	2.0	9.6	6.24	0.538	Plunging	Plunging	3.14

at the toe of the slope, T is the wave period, and x_b is the distance of the breaking point from the toe of the slope. The definition of the breaking point in the present study is the position where wave height reaches its maximum value just before breaking. As the snapshots shown in Fig. 5, the observed breaker type is consistent with the classified one by ξ_0.

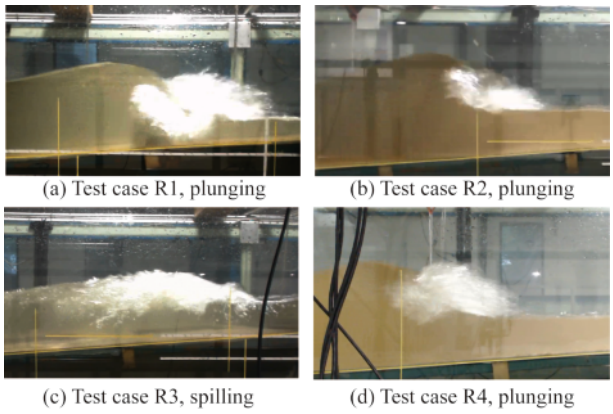

Fig. 5. Snapshots of breaking waves in all test cases.

4 Results and discussion

4.1 Time series of the bed shear stress on the slope under breaking waves

The method of discriminating the direction of the bed shear stress is based on the synchronously measured velocity above the shear stress sensor. Firstly, the bed shear stress in the wave boundary layer has a phase lead which is smaller than 45° over the free-stream flow, and the phase lead will become slight in the very near region above the bed. Secondly, the peak value and duration of velocity in the onshore and offshore direction near the bottom can also be used to distinguish the direction. Under violent breaking with strong air entrainment in the surf zone, both signals of the ADV and shear sensor are disturbed by bubbles. The turbulence and vortexes generated by breaking waves also bring some uncertainty in the direction determination. In the sections where the signal of ADV was severely disturbed, only the absolute value of the bed shear stress $|\tau_b|$ was recorded.

The time series of the bed shear stress on each section along the slope in test cases R1–R3 is shown in Fig. 6. Owing to the reasons mentioned above, not all the directions of the section are resolved. In the present study, the form of incident waves monitored at the toe of the slope is practically constant. As seen from Fig. 6, for regular waves, the bed shear stress is dominated by periodic forms in both outside and inside the breaking point, even though the partial periods after breaking have a slight shift.

The difference between outside and inside the breaking point is clear. Before the breaking point (first row of Fig. 6), no obvious turbulent signal is found. The positive (onshore direction) bed shear stress is larger than the negative (offshore direction) bed shear stress, which is caused by the shoaling process of the incident waves. The asymmetry of the bed shear stress during one wave period is essential to the direction of the bed load transport. After waves breaking, the fluctuations of the bed shear stress increase significantly due to the turbulence and vortexes generated by break-

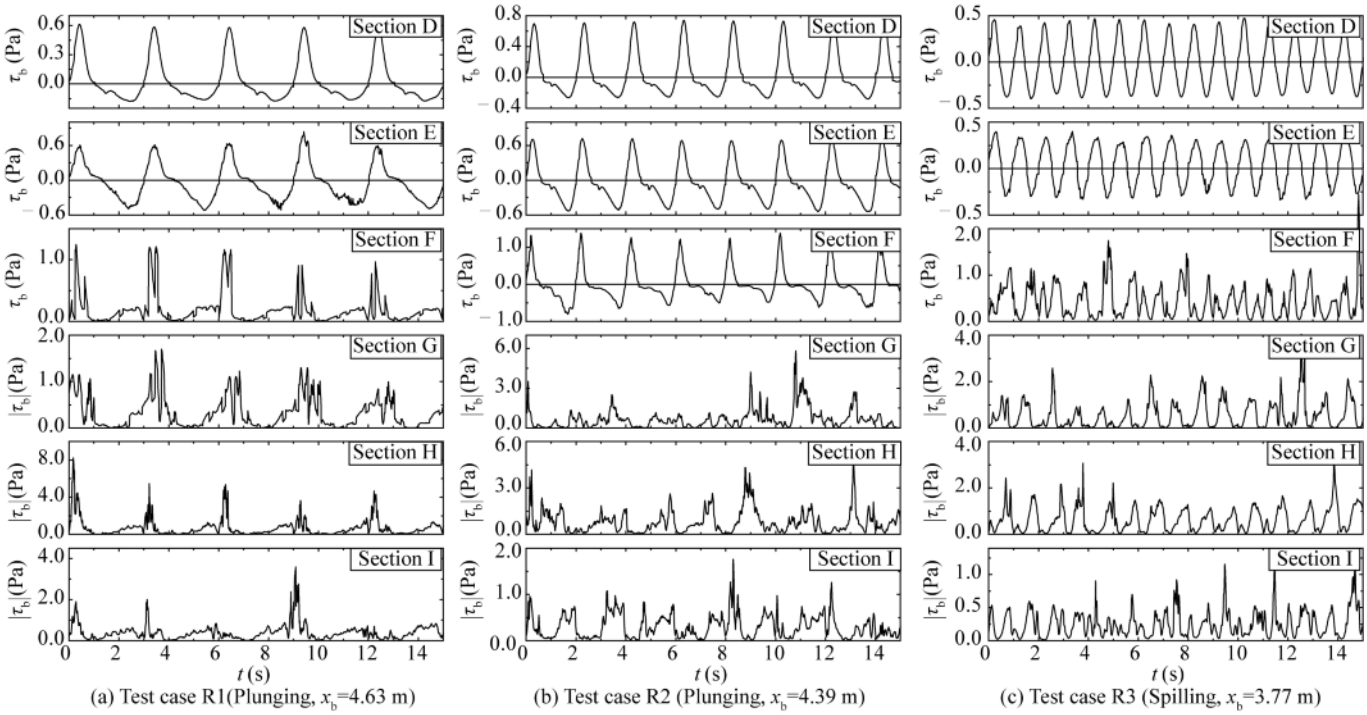

Fig. 6. Time series of the bed shear stress on each section in test cases R1–R3.

ing waves. For plunging breaker (Fig. 6a and 6b), the turbulent signals are more pronounced than the spilling breaker (Fig. 6c). Multi organized peaks appear during one wave period after plunging breaking, which can be clearly observed in Fig. 6a. The plunging jet generated by plunging breaker leads to the penetration of turbulence and organized vortexes into the wave boundary layer (corresponding to snapshot in Fig. 5a), which have a significant effect on the time series of the bed shear stress.

4.2 Distribution of the bed shear stress along the slope under breaking waves

The separation of measured quantity into "wave motion" and "turbulence" is difficult in the surf zone. As the result of the time series described before, the bed shear stress is practically periodic in the surf zone. Hence an ensemble-averaging procedure is used to calculate the mean bed shear stress in one wave period in the present study for regular waves. The mean value of the bed shear stress is calculated through ensemble-averaging defined as:

$$\overline{\tau_{\mathrm{b}}}(t)=\frac{1}{N}\sum_{i=1}^{N}\tau_{\mathrm{b}}[t+(i-1)T], \tag{5}$$

where t is time, $\overline{\tau_{\mathrm{b}}}(t)$ is the mean value of the bed shear stress at time t in one period, N is the number of waves sampled, and T is the wave period. For the sections where the direction of the bed shear stress is not resolved, τ_{b} is replaced with $|\tau_{\mathrm{b}}|$ in Eq. (5). Fig. 7 shows the time variation of the mean bed shear stress in one wave period for each section along the slope.

Note that due to the lack of the direction in latter sections (e.g. Sections G-I in Fig. 7) and the slight shift of the wave period after wave breaking, some periodic local peak values and zero-crossing points will be "submerged" during the ensemble averaging procedure. Before wave breaking (e.g. Sections B-D in Fig. 7), the bed shear stress is governed by the wave boundary layer, and there are no dramatic changes in the bed shear stress to be found. For plunging breaker, the asymmetry of the onshore and offshore in the duration and the peak value of the bed shear stress are larger than those of the spilling breaker before breaking. The duration of the onshore bed shear stress is shorter than the offshore direction. However, the absolute value of the onshore bed shear stress is larger than that of the offshore direction. After breaking, the fluctuation of the mean bed shear stress in plunging case is also larger than that of the spilling case. For spilling breaker, the time variation of the mean shear stress is moderate after wave breaking (seen in Sections F-I of Fig. 7c).

The mean value of the maximum bed shear stresses $|\tau_{\mathrm{m}}|$ is defined as follows:

$$|\tau_{\mathrm{m}}|=\frac{1}{N}\sum_{i=1}^{N}\left|\tau_{\mathrm{b,max}}\right|, \tag{6}$$

where $|\tau_{\mathrm{b,\,max}}|$ is the maximum bed shear stress during each wave period, and N is the number of waves sampled. Fig. 8 shows the cross-shore distribution of the mean value of the maximum bed shear stresses, and the trend of distribution is clear along the slope.

Comparing Fig. 7 with Fig. 8, the maximum bed shear

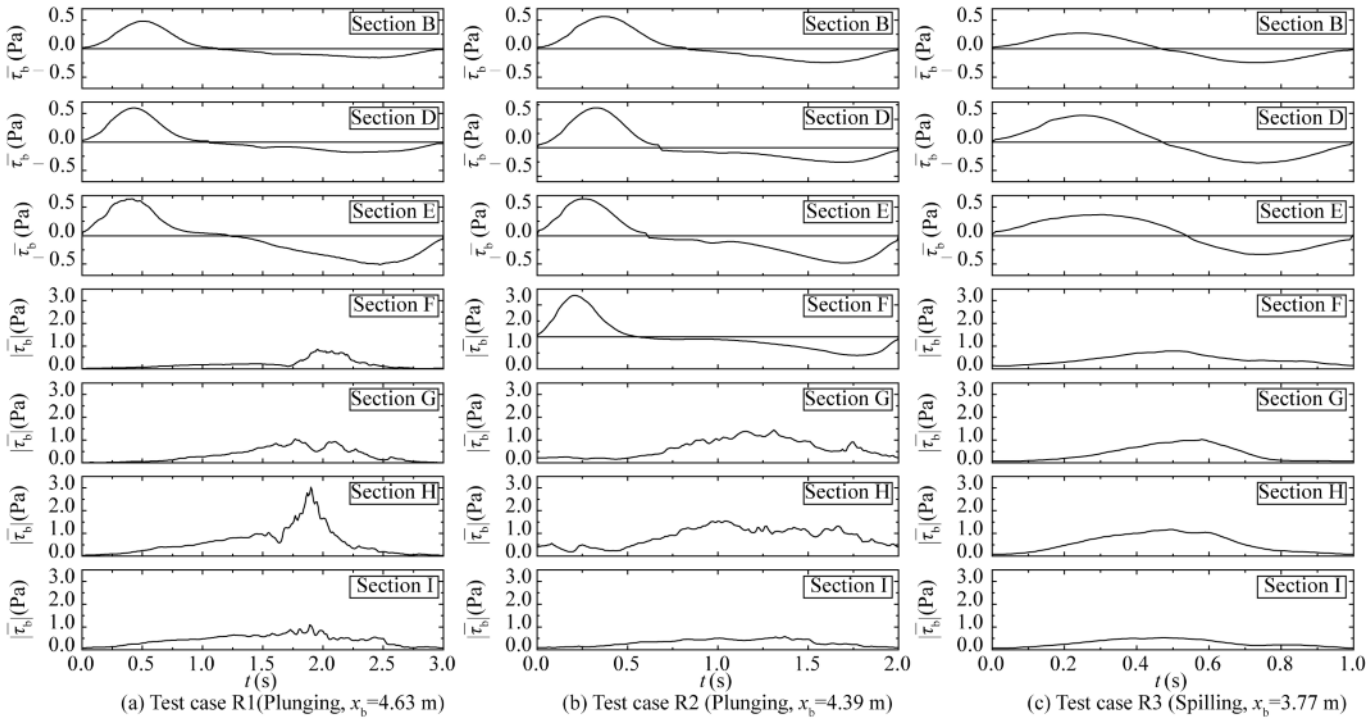

Fig. 7. Time variation of the mean bed shear stress during one period along the slope.

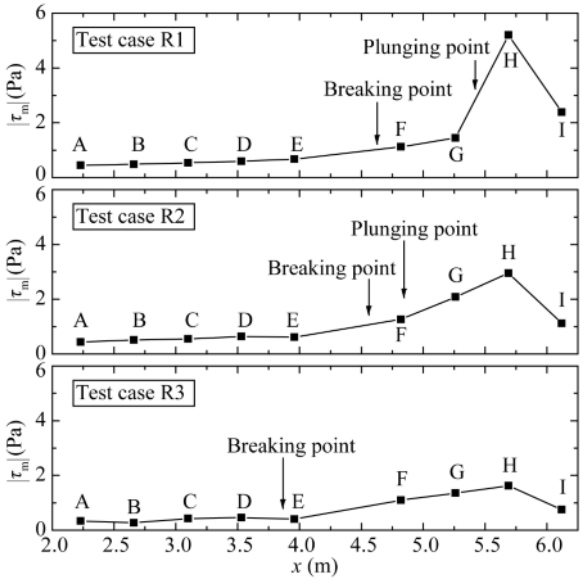

Fig. 8. Cross-shore distribution of the mean values of the maximum bed shear stresses along the slope.

stress calculated by Eq. (6) is larger than the ensemble-averaging one after wave breaking. The reason for this situation is the "submerged" issue mentioned before when performing the ensemble-averaging procedure. As seen from Sections A-D in Fig. 8, changes of the mean value of the maximum bed shear stress along the slope are small outside the breaking point, and the mean value of the maximum bed shear stress has an increasing trend towards the breaking point in both plunging case and spilling case. After wave breaking, the variation of the maximum bed shear stress is considerable. The more violent the wave breaking, the more significant increase of the maximum bed shear stress will occur.

As shown in Fig. 8, the extreme value of the maximum bed shear stress occurs at a distance from the breaking point. For plunging breaker, the extreme value occurs after the plunging point where the plunger falls into the water according to the video recorded, hence the extreme value is a sign of the plunger or the vortex generated by the plunging motion that penetrates into the wave boundary layer. Unlike the dramatic changes in plunging breaker, for spilling breaker, the increase of the maximum bed shear stress is gradual. It indicates that the influence of the surface roller generated by spilling breaker concentrate mainly above the wave boundary layer until the water depth reduced to a certain extent (related to Fig. 5c), and the influence of the moving roller on the bed shear stress is somewhat dominated by water depth in the present study.

4.3 Relationship between the maximum bed shear stress and wave parameters

The precise quantitative analysis is difficult in the surf zone after wave breaking due to the high nonlinearity and turbulence of breaking wave hydrodynamics. In the design of the wave flume experiment, the incident wave height H, wave period T, and water depth h are the key parameters commonly used. Neglecting the effect of viscosity, the relationshiop between the mean value of the maximum bed shear stresses $|\tau_m|$ and the possible involved parameters can be expressed as:

$$F_1(|\tau_m|,\rho,g,h,H,T,\tan\beta)=0, \tag{7}$$

where g is the gravitational acceleration. For most common situation, the deep-water quantities are more convenient to use. According to the linear dispersion relation and the conservation assumption of energy flux (Fredsøe and Deigaard, 1992), parameters H and T can be replaced by H_0 and L_0. Eq. (7) can be rewritten as:

$$F_2(|\tau_m|,\rho,g,h,H_0,L_0,\tan\beta)=0. \tag{8}$$

Considering Eq. (4), parameters H_0, L_0, and $\tan\beta$ can be combined into surf similarity parameter ξ_0. Parameters $|\tau_m|$, ρ, g, and h can be reorganized into the non-dimensional maximum bed shear stress $|\tau_m|/(\rho gh)$. Then Eq. (8) is rearranged into

$$F_3\left(\frac{|\tau_m|}{\rho gh},\frac{\tan\beta}{\sqrt{H_0/L_0}}\right)=0. \tag{9}$$

Hence, the non-dimensional maximum bed shear stress $|\tau_m|/(\rho gh)$ will have a function depending on ξ_0:

$$\frac{|\tau_m|}{\rho gh}=f(\xi_0). \tag{10}$$

From the literature reviewed, only a few direct measured data are available for breaking waves. The measured data from the present study, Deigaard et al. (1991), and Sumer et al. (2013) are plotted in Fig. 9 with logarithmic coordinate. The surf similarity parameter ξ_0 of measured data ranges from 0.189 to 1.420, including spilling breaker and plunging breaker. The dash line ($\xi_0 = 0.5$) in the middle of the figure represents the boundary of spilling and plunging. The non-dimensional maximum bed shear stress increases with the surf similarity parameter. From the discussion in Sections 4.1 and 4.2, surf similarity parameter ξ_0 can be considered as the level of wave breaking influence on the bed shear stress.

After performing a least-square fitting using power

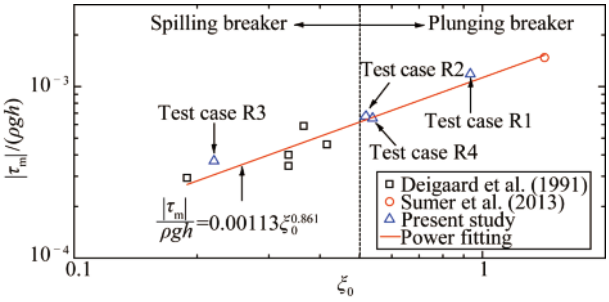

Fig. 9. Relationship between the non-dimensional maximum bed shear stress and the surf similarity parameter.

function, the following empirical equation can be obtained:

$$|\tau_m| = 0.00113\rho g h \zeta_0^{0.861}. \quad (11)$$

Empirical Eq. (11) can be used to estimate the maximum bed shear stress under breaking waves in practice such as the laboratory study for $0.189<\xi_0<1.420$. Attention should be paid that Eq. (11) can only be used on a smooth and constant slope. The morphology and bottom roughness will also have influence on the bed shear stress.

5 Conclusions

Direct measurement of the bed shear stress under breaking waves in the surf zone has been rarely reported due to the lack of effective and accurate means of the measurement in complicated hydrodynamics. A wave flume experiment was carried out to investigate the bed shear stress under regular waves plunging and spilling on a slope by applying a novel instrument named MEMS flexible hot-film shear stress sensor. The following conclusions are drawn from the experimental investigation.

(1) The MEMS flexible hot-film shear stress sensor is feasible for the measurement of the bed shear stress under breaking waves. Before application of the bed shear stress sensor, a careful calibration is required.

(2) For regular waves, the bed shear stress is mainly periodic in both outside and inside the breaking point. After waves breaking, the fluctuations of the bed shear stress increase significantly due to the turbulence and vortexes generated by breaking waves. For plunging breaker, the turbulent signals are more pronounced than those of the spilling breaker, and the plunging jet leads to the penetration of turbulence and vortexes into the wave boundary layer, which has a significant effect on the time series of the bed shear stress.

(3) Changes in the mean value of the maximum bed shear stresses along the slope are small outside the breaking point. The extreme value of the maximum bed shear stress occurs at a distance from the breaking point. For plunging breaker, the extreme value occurs after the plunging point, and the more violently the wave breaks, the more dramatic increase of the maximum bed shear stress will occur. For spilling breaker, the increase of the maximum bed shear stress is gradual compared with the plunging breaker along the slope.

(4) In the present study, an empirical equation about the relationship between the maximum bed shear stress and the surf similarity parameter for smooth and constant slope is given based on the measured data, which can be used to estimate the maximum bed shear stress under breaking waves in practice.

Acknowledgements

The authors gratefully acknowledge the research team of Prof. MA Bing-he from Northwestern Polytechnical University for providing the MEMS flexible hot-film shear stress sensor and the engineering prototype. We would like to thank Prof. Jørgen Fredsøe and Dr. Nilas Mandrup Hansen for providing some of the literature.

References

Barnes, M.P., O'Donoghue, T., Alsina, J.M. and Baldock, T.E., 2009. Direct bed shear stress measurements in bore-driven swash, *Coastal Engineering*, 56(8), 853–867.

Boers, M., 2005. *Surf Zone Turbulence*, Ph.D. Thesis, Delft University of Technology, Netherlands.

Carstensen, S., Sumer, B.M. and Fredsøe, J., 2010. Coherent structures in wave boundary layers. Part 1. Oscillatory motion, *Journal of Fluid Mechanics*, 646, 169–206.

Cox, D.T., Kobayashi, N. and Okayasu, A., 1996. Bottom shear stress in the surf zone, *Journal of Geophysical Research*, 101(C6), 14337–14348.

Deigaard, R., Mikkelsen, M.B. and Fredsøe, J.,1991. *Measurements of the Bed Shear Stress in A Surf Zone*, Prog. Rep. 73, Institute of Hydrodynamics and Hydraulic Engineering, Technical University of Denmark, Lyngby, 21–30.

Fredsøe, J. and Deigaard, R., 1992. *Mechanics of Coastal Sediment Transport*, World Scientific Publishing Company, Singapore.

Fredsøe, J., Sumer, B.M., Kozakiewicz, A., Chua, L.H.C. and Deigaard, R., 2003. Effect of externally generated turbulence on wave boundary layer, *Coastal Engineering*, 49(3), 155–183.

Galvin, C.J.Jr., 1968. Breaker type classification on three laboratory beaches, *Journal of Geophysical Research*, 73(12), 3651–3659.

Hanratty, T.J. and Campbell, J.A., 1996. Measurement of wall shear stress, in: Goldstein, R.J. (ed.), *Fluid Mechanics Meaurements*, 2nd ed., Taylor & Francis, Washington, D.C., 575–648.

Huang, H.L., Zuo, Q.H., Zhou, Y.R., Shen, Y.S. and Li, L.X., 2016. Design of measuring instrument with whole direct method for bed shear stress under two-dimensional water-flow co-action, *China Ocean Engineering*, 30(6), 916–925.

Hultmark, M. and Smits, A.J., 2010. Temperature corrections for constant temperature and constant current hot-wire anemometers, *Measurement Science and Technology*, 21(10), 105404.

Huo, G., Wang, Y.G., Yin, B.S. and You, Z.J., 2007. A new measure for direct measurement of the bed shear stress of wave boundary layer in wave flume, *Journal of Hydrodynamics*, *Ser. B*, 19(4), 517–524.

Jensen, B.L., Sumer, B.M. and Fredsøe, J., 1989. Turbulent oscillatory boundary layers at high Reynolds numbers, *Journal of Fluid Mechanics*, 206, 265–297.

Knight, D.W., Demetriou, J.D. and Hamed, M.E., 1984. Boundary shear in smooth rectangular channels, *Journal of Hydraulic Engineering*, 110(4), 405–422.

Ma, B.H., Ren, J.Z., Deng, J.J. and Yuan, W.Z., 2010. Flexible thermal sensor array on PI film substrate for underwater applications, *Proceedings of the 23rd International Conference on Micro Electro Mechanical Systems* (*MEMS*), IEEE, Wanchai, Hong Kong, 679–682.

Mirfenderesk, H. and Young, I.R., 2003. Direct measurements of the bottom friction factor beneath surface gravity waves, *Applied Ocean Research*, 25(5), 269–287.

Musumeci, R.E., Marletta, V., Andò, B., Baglio, S. and Foti, E., 2015. Measurement of wave near-bed velocity and bottom shear stress by ferrofluids, *IEEE Transactions on Instrumentation and Measurement*, 64(5), 1224–1231.

Pujara, N. and Liu, P.L.F., 2014. Direct measurements of local bed

shear stress in the presence of pressure gradients, *Experiments in Fluids*, 55, 1767.

Schlichting, H. and Gersten, K., 2017. *Boundary-layer Theory*, 9th ed., Springer, Berlin.

Seelam, J.K., Guard, P.A. and Baldock, T.E., 2011. Measurement and modeling of bed shear stress under solitary waves, *Coastal Engineering*, 58(9), 937–947.

Soulsby, R., 1997. *Dynamics of Marine Sands*: *A Manual for Practical Applications*, Thomas Telford, London.

Sumer, B.M., Arnskov, M.M., Christiansen, N. and Jørgensen, F.E., 1993. Two-component hot-film probe for measurements of wall shear stress, *Experiments in Fluids*, 15(6), 380–384.

Sumer, B.M., Sen, M.B., Karagali, I., Ceren, B., Fredsøe, J., Sottile, M., Zilioli, L. and Fuhrman, D.R., 2011. Flow and sediment transport induced by a plunging solitary wave, *Journal of Geophysical Research*, 116(C1), C01008.

Sumer, B.M., Guner, H., Hansen, N.M., Fuhrman, D.R. and Fredsøe, J., 2013. Laboratory observations of flow and sediment transport induced by plunging regular waves, *Journal of Geophysical Research*: *Oceans*, 118(11), 6161–6182.

Xu, H., Xia, Y.F., Ma, B.H., Hao, S.Y., Zhang, S.Z. and Du, D.J., 2015. Research on measurement of bed shear stress under wave-current interaction, *China Ocean Engineering*, 29(4), 589–598.

Yüksel, Y., Çevik, E.Ö. and Kapdanşli, S., 1998. Bed shear stress distribution over beach profiles, *Journal of Coastal Research*, 14(3), 1044–1053.

You, Z.J. and Yin, B.S., 2007. Direct measurement of bottom shear stress under water waves, *Journal of Coastal Research*, 50, 1132–1136.